Journal of Materials Chemistry

www.rsc.org/materials

Volume 22 | Number 16 | 28 April 2012 | Pages 7635–8146

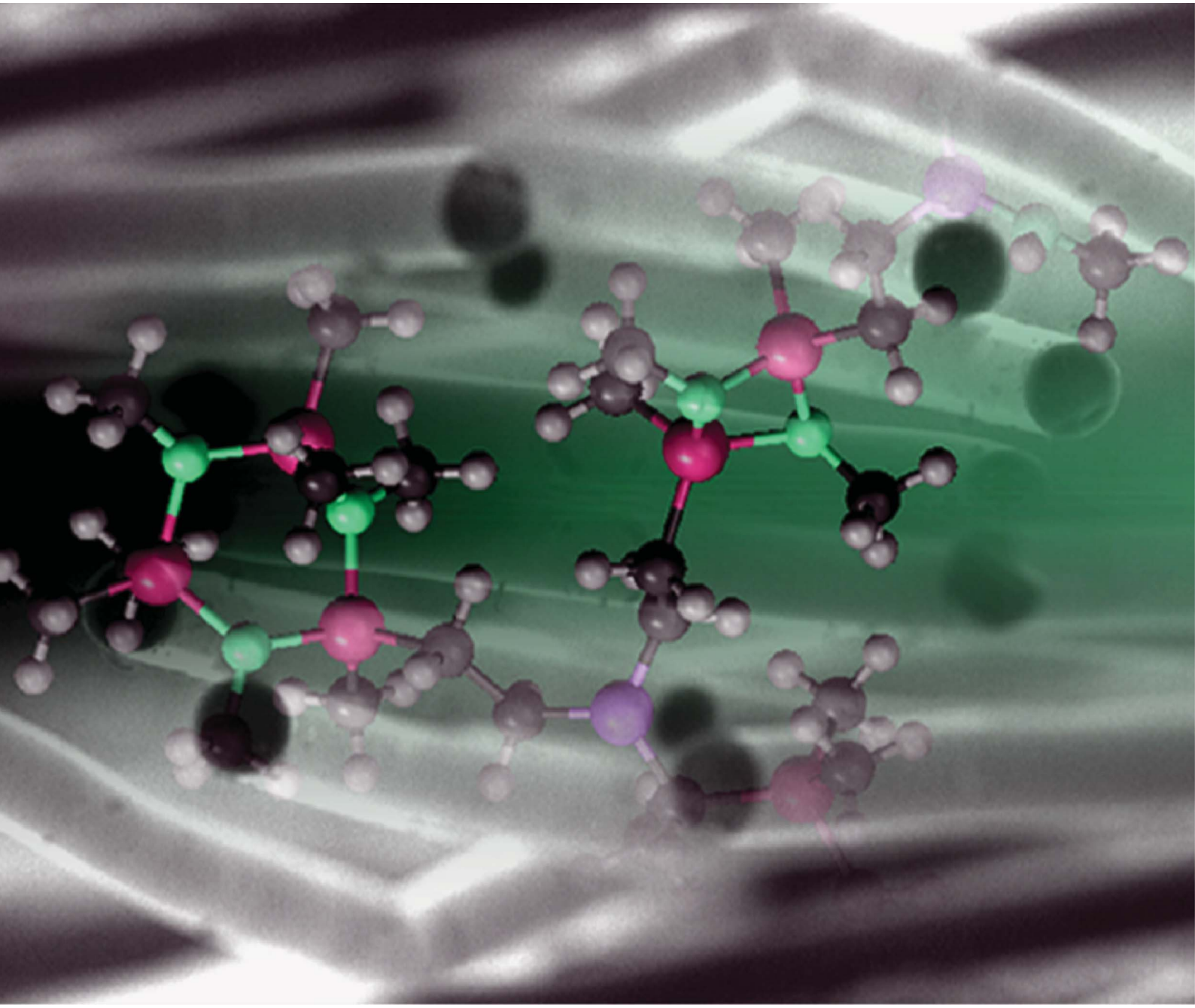

ISSN 0959-9428

RSC Publishing

PAPER

Laura Gottardo *et al.*

Chemistry, structure and processability of boron-modified polysilazanes as tailored precursors of ceramic fibers

Journal of Materials Chemistry

Dynamic Article Links

Cite this: J. Mater. Chem., 2012, 22, 7739

www.rsc.org/materials

PAPER

Published on 08 March 2012. Downloaded by UNIVERSITAT BAYREUTH on 9/4/2020 6:13:40 AM.

Chemistry, structure and processability of boron-modified polysilazanes as tailored precursors of ceramic fibers†

Laura Gottardo,‡[a] Samuel Bernard,*[a] Christel Gervais,[b] Kathrin Inzenhofer,[c] Günter Motz,[c] Markus Weinmann,[d] Corneliu Balan[e] and Philippe Miele[a]

Received 16th November 2011, Accepted 7th February 2012
DOI: 10.1039/c2jm15919h

A series of boron-modified polysilazanes (BmPSs) of the type $[B(C_2H_4SiCH_3NCH_3)_3]_n$ was synthesized by reaction of tris(dichloromethylsilylethyl)borane ($B(C_2H_4SiCH_3Cl_2)_3$, TDSB) with methylamine (MA) using various MA : TDSB ratios and then characterized for suitability as precursors of Si/B/C/N ceramic fibers. Molecular chemistry and polymer structure of BmPSs are investigated in the present paper by elemental analyses, solid-state NMR and molecular weight measurements. It is shown that the MA : TDSB ratio fixed during the polymer synthesis strongly modifies the proportion of identified structural units, determines the boron environment and influences the molecular weight of polymers, causing different responses to melt-spinnability. Based on fiber shape visualization using a CCD camera during extrusion and stretching, appropriate melt-spinnable compounds are prepared with MA : TDSB ratios between 9.0 and 9.2. These polymers represent structurally complex networks composed of four- and/or six-membered $-(Si-N)_n-$ rings bridged *via* tri-coordinated $BC_{3-x}N_x$ and tetra-coordinated $BC_{4-x}N_x$ units. In such polymers, the proportion of terminal $N(H)CH_3$ groups as well as the $BC_{3-x}N_x$: $BC_{4-x}N_x$ ratio are especially tailored for melt-spinning. Such compounds display a chemical formula of $[Si_{3.0}B_{1.1}C_{11.35\pm0.5}N_{3.8\pm0.4}H_{8.15\pm1.35}]_n$ with $n \approx 2.5$. They have a glass transition temperature of 48 ± 4 °C, tailored flexibility and sufficient plasticity to successfully produce fine-diameter green fibers at 107 ± 8 °C in a stable melt-spinning process. After melt-spinning, green fibers have been cured then pyrolyzed up to 1000 °C to generate silicoboron carbonitride ($Si_{3.0}B_{1.0}C_{5.0}N_{2.4}$) fibers with 10–13 μm in diameter according to an established procedure. Polymer fibers have a ceramic yield of 44% after thermal decomposition at 1000 °C. The circular fibers exhibit a dense texture with a glassy section, indicating an amorphous state of the ceramic which was further confirmed by TEM as well as Weibull strengths of 1.4 GPa and Young's modulus of 120 GPa.

1 Introduction

The Polymer-Derived Ceramics (PDCs) route was introduced in the first half of the 60's[1] and widely developed in the 70's through the introduction of silicon nitride/silicon carbide (Si_3N_4/SiC) and SiC fibers.[2,3] It is based on the shaping and subsequent pyrolysis of preceramic polymers.[4–29] It offers significant benefits over traditional ceramic processing techniques to prepare ceramics including the design of the atomic structure, nanostructuration of the material and possibility to prepare net-shape components.[7–10] The PDC route represents a synthetic approach in which the chemistry of molecular precursors and preceramic polymers is designed on the atomic scale to deliver the desired inorganic polymer composition. Such polymers may be processable to produce a large variety of materials in particular shapes that are difficult or even impossible to obtain by conventional powder processing. As examples, it is now possible to produce complex compositional systems[11] and nanocomposites[12] for the preparation of multifunctional ceramics, ceramics with controlled porosity for filtration and/or energy technologies,[13–18] and a large variety of shaped ceramics going from 0D to 3D such as particles and spheres,[19,20] (nano) fibers,[21–23] coatings,[24] bulk parts[25,26] and composites[27] for a large range of application fields. More specific and original shapes including MEMS[28] and microfluidic systems[29] can also be

[a]*Institut Européen des Membranes (UMR CNRS 5635), IEM/Université Montpellier 2, CC047—Place E. Bataillon, 34095 Montpellier Cedex 5, France. E-mail: Samuel.Bernard@iemm.univ-montp2.fr*
[b]*Laboratoire de Chimie de la Matière Condensée UMR CNRS 7574, UPMC Univ Paris 06, Collège de France, 11 Place M. Berthelot, 75005 Paris, France*
[c]*University of Bayreuth, 95440 Bayreuth, Germany*
[d]*H. C. Starck GmbH, Im Schleeke 78-91, D-38642 Goslar, Germany*
[e]*REOROM Laboratory, Hydraulics Department, "Politehnica" University of Bucharest, Splaiul Independentei 313, 060042 Bucharest, Romania*
† Electronic supplementary information (ESI) available. See DOI: 10.1039/c2jm15919h
‡ Present address: EMPA, Laboratory for Advanced Fibers, 5 Lerchenfeldstrasse CH-9014 St. Gallen, Switzerland.

Published on 08 March 2012. Downloaded by UNIVERSITAT BAYREUTH on 9/4/2020 6:13:40 AM.

produced. Therefore, this method offers versatility which allows us to prepare the desired material for the targeted application.

Processing of Si-based ceramic fibers including SiC, Si_3N_4, silico carbonitride (Si/C/N) and silicoboron carbonitride (Si/B/C/N) derived from preceramic polymers such as polycarbosilanes (PCSs), polysilazanes, polycarbosilazanes and boron-modified polysilazanes or polyborosilazanes[30–42] is still an extremely challenging topic in PDCs. They represent the best candidate to reinforce a ceramic matrix in the next generation of nuclear energy conversion power plants. These fibers can be defined as materials in elongated form with a circular section having small diameters (<20 μm), high aspect ratio, good tensile strengths (σ = 2 GPa) and a low density ($d \leq 3$ g cm^{-3}). Production of PDC fibers (PDCFs) is based on a four-step sequence for which each step has specific requirements: (1) synthesis of preceramic polymers from molecular precursors → (2) spinning of the polymer (in solution or in the molten state) → (3) imposed crosslinking (= curing) of green fibers → (4) pyrolysis of crosslinked fibers into a ceramic object with retention of the imposed shape.

Controlling the various requirements, *i.e.*, fusibility, stability at low temperature for melt-spinning, sufficient ceramic yield and so on, and combining them in only one polymer remains an ambitious objective. The choice of the preceramic polymer, *i.e.*, the structure of the polymer backbone and the attached functional groups or substituents, has to be done with extreme caution to find a compromise between all requirements. This is illustrated in Fig. 1 which shows a polysilazane in which different substituents R, R′ and R″ are linked to the polymer backbone.

The substituents strongly influence processing properties of the polymer upon melt-spinning, ceramic yields and the final ceramic composition. For example, SiCH=CH_2, SiH and NH groups offer the opportunity to attach supplementary elements to the polymer skeleton. Boron, for example, may be introduced by hydroboration of CH=CH_2 groups using borane Lewis base adducts.[40] Accordingly the molecular weights of polymers may be increased *via* hydrosilylation (SiH + SiCH=CH_2).[40] Reactions may involve deshydrocoupling with formation of Si–N units (SiH + NH).[43] In contrast, Si- and N-bounded substituents such as methyl or ethyl are chemically inert and are usually introduced to adjust the needed physical and chemical properties, *e.g.* to optimize the spinning behavior[44] and to adjust the thermal degradation.[45] It is therefore worth mentioning that properties of PDCs and in particular PDCFs are strongly related to their molecular origin. As a consequence, the molecular structure and chemistry of preceramic polymers have to be tailored to produce ceramics endowed with designed performance properties that go far beyond those of existing materials.

Ceramics based on the quaternary system Si/B/C/N have been recently discovered.[46–48] They are highly durable and display properties targeted at applications using advanced materials

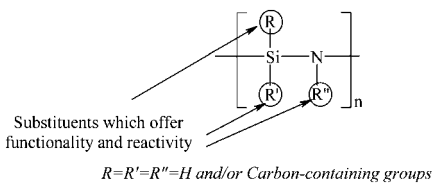

Fig. 1 Schematic representation of a polysilazane structure.

enabling high-efficiency use of energy resources which exert a minimal burden on the environment and that will help energy conservation. For example, Si/B/C/N fiber-matrix[46–48] composites have the potential to be applied in heat engines (*e.g.* turbines) as well as in the next generation nuclear energy conversion power plants.

In particular, the Si/B/C/N fibers studied in the present paper represent high-temperature stable amorphous ceramic fibers.[36] They remain amorphous even after annealing at 1700 °C in a nitrogen atmosphere which represents a great improvement in comparison to classical Si-containing ceramic fibers including SiC, Si_3N_4 and Si/C/N fibers which are stable under the same conditions up to 1400–1500 °C. Initial work for the preparation of Si/B/C/N fibers was done by Takamizawa *et al.* in 1986.[49] Ceramic fibers of 11 μm in diameter, 3.0 GPa in tensile strength and 250 GPa in Young's modulus were produced. These fibers remained amorphous up to 1500 °C in a nitrogen environment and their tensile strength was maintained at 2.0 GPa at this temperature. Lu *et al.* elaborated Si/B/C/N fibers which were thermally stable up to 1600 °C.[50a,b] More recently,[50c] they investigated the production of Si/B/C/N(O) fibers of 15.6 mm in diameter and 1.6 GPa in tensile strength but the synthesis procedure, *i.e.* physical mixing of different polymers or heterogeneous introduction of elements during the curing and pyrolysis, did not lead to ideal compositional and structural homogeneities in the final ceramic involving poorer thermal stability than Si/B/C/N fibers produced from single-source precursors like those studied in the present paper. Following this approach, Sneddon *et al.* described polymer-derived Si/B/C/N fibers which were amorphous at 1600 °C.[51] Jansen *et al.* prepared *N*-methyl polyborosilazanes tailored to be meltable and spinnable by melt- or solution-spinning processes.[33] The resulting green fibers were cured and pyrolyzed up to 1500 °C. Amorphous Si/B/C/N fibers remained thermally stable up to 1750 °C in a non-oxidizing atmosphere (0.1 MPa, He).

The Si/B/C/N fibers reported in the present paper crystallize slightly earlier than those produced by Jansen *et al.* which is probably related to the molecular configuration of boron-modified polysilazanes (BmPSs) that exhibit B–C bonds, whereas *N*-methyl polyborosilazanes have only B–N bonds. In addition, Si/B/C/N fibers produced from BmPSs are obtained at lower temperature (1000 °C) which is less time-consuming and they display a mean strength of 1.3 GPa which is higher than 0.75 GPa which has been recently reported for Si/B/C/N fibers produced from *N*-methyl polyborosilazanes[52] and they appear to be the most stable in air.[36] According to these properties, they display potentialities for applications at high temperature and under harsh environment.

The development of their tailor-made material properties requires an interdisciplinary base that spans the fields of molecular chemistry, chemistry of materials and materials science. At first, a detailed investigation into the polymer chemistry is required. Second, the control of the polymer-to-ceramic conversion through various metastable intermediates and the use of isothermal treatments at selected temperatures must be performed with a general and detailed understanding to generate materials with the desired nano- or microstructure. Finally, as-obtained materials have to be characterized for the targeted application.

 This journal is © The Royal Society of Chemistry 2012

Published on 08 March 2012. Downloaded by UNIVERSITAT BAYREUTH on 9/4/2020 6:13:40 AM.

In the present work, individual steps of the process depicted in Fig. 2 have been carefully investigated. In particular, we describe the synthesis of a series of BmPSs of the type $[B(C_2H_4SiCH_3NCH_3)_3]_n$ by the reaction of methylamine (MA) as a network building agent with tris(dichloromethylsilylethyl) borane (TDSB) as a molecular precursor using different MA : TDSB ratios. As-obtained BmPSs were fully chemically and structurally characterized and then tested with regard to melt-spinning to form green fibers. Melt-spinnable compounds have been selected according to their MA : TDSB ratio and spun into green fibers which were cured under ammonia at 200 °C to render them infusible. The fibers were finally pyrolyzed under nitrogen at 1000 °C to yield $Si_{3.0}B_{1.0}C_{5.0}N_{2.4}$ ceramic fibers (Fig. 2).

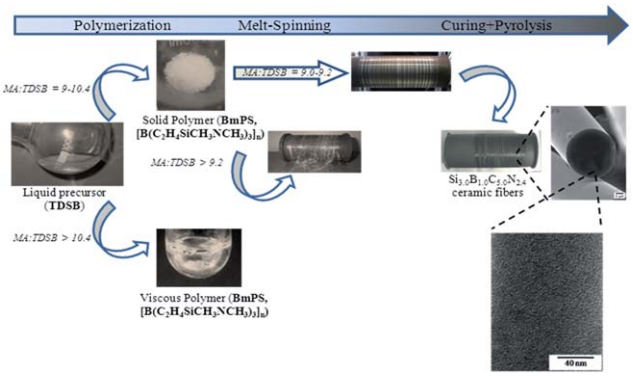

Fig. 2 Overall synthetic path employed to generate $Si_{3.0}B_{1.0}C_{5.0}N_{2.4}$ fibers from BmPSs.

The molecular chemistry and the structure of the polymers were investigated by means of elemental analyses, ^{11}B, ^{13}C, ^{29}Si solid-state NMR spectroscopy and molecular weight measurements. The spinning behavior of BmPSs was monitored using CCD camera visualization of fiber geometry during extrusion and fiber stretching. We therefore provided synthesis conditions that allow us to select the most appropriate polymers for melt-spinning. In a subsequent process, these fibers have been cured and then pyrolyzed to be transformed into Si/B/C/N fibers. Their thermal decomposition as well as their microstructural organization and mechanical behavior have been investigated.

2 Experimental section

2.1. General comment

All synthesis reactions were carried out in a purified argon atmosphere passing through successive columns of BTS-catalyst and phosphorus pentoxide by means of standard Schlenk techniques. Dichloromethylvinylsilane (DMVS, $CH_2{=}CHSiCH_3Cl_2$) was obtained from Sigma-Aldrich and freshly distilled from magnesium at 115 °C at p_{atm} before use. Borane dimethylsulfide $BH_3{\cdot}S(CH_3)_2$ (2 M solution in toluene) was obtained from Sigma-Aldrich and used without further purification. Methylamine (MA) anhydrous (Sigma-Aldrich, 99+%) was used as-received. Tetrahydrofuran (THF) and toluene were purified by distillation from sodium using benzophenone. All chemicals were handled inside an argon-filled glove box (Jacomex BS521) in a dried atmosphere (phosphorus pentoxide).

2.2. Sample characterization

As the polymers are reactive towards moisture and oxygen, the following sample preparations were performed within an argon-filled glove box.

The chemical structure of the polymers was determined by a FT-IR spectrophotometer using a Nicolet Magna 550 Fourier transform-infrared spectrometer in a KBr matrix (dried at 120 °C in air). ^1H and ^{13}C NMR spectra of polymer solutions were obtained using a Bruker AM 300 spectrometer in $CDCl_3$ operating at 300 MHz and 62.5 MHz, respectively. Tetramethylsilane (TMS) was used as a reference for the NMR data. Solid-state ^{13}C, ^{29}Si and ^{11}B MAS NMR spectra were recorded respectively at 100.61, 59.63 and 128.28 MHz, respectively on a Bruker AVANCE 400 spectrometer (9.4 T) using 4 mm Bruker probes and spinning frequencies of 12 kHz. Chemical shift values were referenced to tetramethylsilane for ^{13}C and ^{29}Si and liquid BF_3OEt_2 for ^{11}B. ^{13}C IRCP MAS experiments were performed under the following Hartmann–Hahn match conditions: both RF channel levels, $\omega_{1S}/2\pi$ and $\omega_{1I}/2\pi$, were set at about 50 kHz. The spectra were simulated with the DMFIT program.[53] Chemical analyses were performed using a combination of several methods. Boron, nitrogen, and hydrogen were analyzed at the Service Central de Microanalyse du CNRS (Vernaison, France), whereas carbon and oxygen contents were determined at SPCTS (Limoges, France). The methods included thermal decomposition of samples under oxygen to measure the hydrogen and carbon contents, under inert atmosphere for the measurement of nitrogen and oxygen contents and by ICP-MS (from Thermo-Fisher) for boron and silicon contents. The gel permeation chromatography (GPC) system equipped with two Styragel HT3 columns (500–30 000 MW range), one Styragel HT4 column (5000–600 000 MW range), and a UV detector (254 nm) was used for molecular weight measurement relative to polystyrene standards. Tetrahydrofuran (THF) was the mobile phase. Glass transition was obtained by a differential scanning calorimeter (DSC, Mettler Toledo DSC TA 8000) in an argon atmosphere between 5 °C and 150 °C at a heating rate of 10 °C min^{-1} in aluminium crucibles. Green fiber pictures were recorded during melt-spinning operation using a Sony DXC-9100P 3CCD camera equipped with a 40× zoom. The camera resolution was 782 × 582 pixels (800 vertical lines × 575 horizontal lines). Precision of the diameter measurements was 1 pixel (<2% of diameter). Thermogravimetric analysis (TGA) of the polymer-to-ceramic conversion was recorded on a Setaram TGA 92 16.18. Experiments were performed using silica crucibles (sample weight ~40 mg) at atmospheric pressure (i) in a nitrogen atmosphere at 1 °C min^{-1} from RT to 1000 °C, (ii) at 0.5 °C min^{-1} to 200 °C, dwelling there for 1 h in flowing ammonia. Ammonia was switched off after 1 h at 200 °C and nitrogen was introduced in the furnace which was held for 1 h at 200 °C then heated to 1000 °C (1 °C min^{-1}), dwelling there for 2 h, and then cooling down to RT at 5 °C min^{-1} at ambient atmospheric pressure. Experimental differential thermogravimetric (DTG) data were generated from TGA measurements. Transmission electron microscopy (TEM) micrographs were obtained using a Topcon EMB-002B microscope (Yokohama, Japan) in both imaging and diffraction modes (diffraction patterns were obtained on 0.5 μm selected areas-SAED patterns) on fragments of fibers embedded

Published on 08 March 2012. Downloaded by UNIVERSITAT BAYREUTH on 9/4/2020 6:13:40 AM.

in an epoxy resin then cut with an ultramicrotome (LEICA S). Samples were characterized using a Philips PW 3040/60 X'Pert PRO X-ray diffraction system. Fibers were firstly crushed then placed on the XRD sample holder (PVC). Cu Kα (λ = 1.54 Å) radiation with a Ni filter was used with a working voltage and a current of 40 kV and 30 mA, respectively. Scans were continuous from 20–90° 2θ with a time per step of 0.85 s in increments of 0.017° 2θ. Tensile tests and diameter values were obtained at room temperature from single filaments with a gauge length of 10 mm. 38 single filaments were taken from bundles throughout to incorporate any possible property variation within the lot in fiber fracture statistics. Each filament was centreline mounted and both tips were glued on special slotted tabs for handling and testing. The diameter ϕ of each filament was measured by laser interferometry in two positions along the filament axis and an average diameter of $Si_{3.0}B_{1.0}C_{5.0}N_{2.4}$ fibers was calculated from the 38 values. Single filament tensile properties were determined using a standard tensile tester (Adamel Lhomargy DY 22) including two grips, a displacement transducer and a load cell (5 N). The cross-head speed was fixed at 0.1 mm min^{-1}. Filament cross-sectional areas (A) were determined from the values of diameters. Failure strain ε, Young's modulus E and tensile strength σ were measured from data of breaking load-elongation curve records and cross-sectional area calculations. Each value of failure strain and Young's modulus was modified with system compliance. The average failure strain and Young's modulus were calculated from the 38 tests. The statistical variability of the strength was reported in terms of Weibull statistics. An average tensile strength σ of $Si_{3.0}B_{1.0}C_{5.0}N_{2.4}$ fibers was then estimated for a failure probability $P = 0.632$.

2.3. Molecular design of BmPSs

BmPSs have been obtained by hydroboration of DMVS $CH_2{=}CHSiCH_3Cl_2$ according to procedures described in the literature[54–56] and subsequent aminolysis with methylamine (MA) of tris(dichloromethylsilylethyl)borane $B(C_2H_4SiCH_3Cl_2)_3$ (TDSB, $C_2H_4{=}CHCH_3$, CH_2CH_2) in THF at 0 °C. MA was trapped in a Schlenk tube in liquid air and accordingly, a corresponding amount of TDSB was precisely adjusted into the Schlenk flask. The Schlenk tube containing MA was connected to the cooled Schlenk flask containing THF solution of TDSB and removed from the liquid air cooling bath. Both parts were linked *via* an interconnection flexible tube which was evacuated and then refilled with argon. Argon was slowly introduced in the Schlenk tube containing MA and, after the central valve was opened, MA was allowed to warm up to RT to be passed through the solution at 0 °C under vigorous stirring. When addition was complete, the mixture was allowed to warm to 25 °C and kept at this temperature under vigorous stirring overnight. The solution was then separated from the precipitate by filtration through a pad of Celite. The solvent was removed by distillation (RT/1.5 × 10^{-1} mbar) to release air- and moisture-sensitive colorless polymers. The reaction between TDSB and MA proceeded quantitatively; the separation from the by-product methylamine hydrochloride by filtration resulted in product loss ≤10%.

Using this general procedure, we synthesized a set of representative BmPSs (**BmPS9.0** → **BmPS10.4**) by deliberately changing the MA : TDSB ratio. Table 1 reports experimental details of the polymerization procedures for each of the polymers which have been prepared.

Polymers were synthesized in the solid state based on the MA : TDSB ratios reported in Table 1. It is important mentioning that a MA : TDSB ratio higher than 10.6 involved a change in the physical state of the polymer and led to viscous boron-modified polysilazanes with viscoelasticities unsuitable for melt-spinning. Therefore, only ratios with 9.0 ≤ MA : TDSB < 10.6 have been predominantly considered in the present study.

BmPS9.0 was obtained with a MA : TDSB ratio of 9.0 as a white powder. Anal. found (wt%): C, 42.33; H, 11.57; N, 14.55; B, 3.6; Si, 26.2; O, 1.72 $[Si_{3.0}B_{1.1}C_{11.3}N_{3.3}H_{36.8}]_n$ ($[317.49]_n$). Calcd C, 46.25; H, 9.70; N, 13.54; B, 3.42; Si, 27.04 $[Si_{3.0}B_{1.0}C_{12.0}N_{3.0}H_{30.0}]_n$. IR (KBr/cm^{-1}): ν(N–H) = 3425, 3321, 3229 w; ν(C–H) = 2954 s, 2898 s, 2803 m; δ(N(H)CH_3) = 1596 w; δ_{asym}(CH_3) = 1463 w; ν(C–C) = 1355 w; δ(Si–CH_3) = 1254 s; δ(C–B–C) = 1187 m; δ(SiCH_2C) = 1139 m; ν(C–N) = 1061 m; δ(N–Si–N) = 914 sh-875 *vs.* ^{1}H NMR ($CDCl_3$) (ppm): δ = 0.12 (br, SiCH_3), δ = 0.21 (vbr, Si$CH_2$$CH_2$B), δ = 0.78 (br, CH_3CHBSi), δ = 1.11 (br, Si$CH_2$$CH_2$B), δ = 1.21 (br, CH_3CHBSi), δ = 2.27 (vbr, NCH_3).

BmPS9.2 was obtained with a MA : TDSB ratio of 9.2 as a powder. Anal. found (wt%): C, 40.81; H, 11.6; N, 15.43; B, 3.51; Si, 25.7; O, 0.68 $[Si_{3.0}B_{1.1}C_{11.8}N_{3.6}H_{37.7}]_n$ ($[326.3]_n$). Calcd C, 46.25; H, 9.70; N, 13.54; B, 3.42; Si, 27.04 $[Si_{3.0}B_{1.0}C_{12.0}N_{3.0}H_{30.0}]_n$. IR (KBr/cm^{-1}): ν(N–H) = 3427, 3320, 3229 w; ν(C–H) = 2953 s, 2895 s, 2805 m; δ(N(H)CH_3) = 1599 w; δ_{asym}(CH_3) = 1462 w; ν(C–C) = 1355 w; δ(Si–CH_3) = 1257 s; δ(C–B–C) = 1181 m; δ(SiCH_2C) = 1139 m; ν(C–N) = 1061 m; δ(N–Si–N) = 912 sh-876 *vs.* ^{1}H NMR ($CDCl_3$) (ppm): δ = 0.10 (br, SiCH_3), δ = 0.21 (vbr, Si$CH_2$$CH_2$B), δ = 0.80 (br, CH_3CHBSi), δ = 1.10 (br, Si$CH_2$$CH_2$B), δ = 1.23 (br, CH_3CHBSi), δ = 2.30 (vbr, NCH_3).

BmPS9.7 was obtained with a MA : TDSB ratio of 9.7 as a powder. Anal. found (wt%): C, 42.76; H, 11.68; N, 15.58; B, 3.32; Si, 24.65; O, 1.91 $[Si_{3.0}B_{1.1}C_{12.2}N_{3.8}H_{39.6}]_n$ ($[335,8]_n$). Calcd C, 46.25; H, 9.70; N, 13.54; B, 3.42; Si, 27.04 $[Si_{3.0}B_{1.0}C_{12.0}N_{3.0}H_{30.0}]_n$. IR (KBr/cm^{-1}): ν(N–H) = 3423, 3321, 3230 w; ν(C–H) = 2954 s, 2899 s, 2805 m; δ(N(H)CH_3) = 1605 w; δ_{asym}(CH_3) = 1462 w; ν(C–C) = 1356 w; δ(Si–CH_3) = 1252 s; δ(C–B–C) = 1187 m; δ(SiCH_2C) = 1136 m; ν(C–N) = 1060 m;

Table 1 Experimental details of the polymerization procedures for each BmPSs

BmPS	TDSB/g mmol^{-1}	MA/g mmol^{-1}	MA : TDSB ratio	V_{THF}/mL	Polymer/g mmol^{-1}
9.0	40.7/93.1	26/837.16	9.0	500	26.6/84.6
9.2	63.3/144.8	40.6/1307.3	9.2	700	42.1/135.3
9.7	24.8/56.7	17.3/557.04	9.7	350	16.6/52.8
10.4	29.1/66.5	21/676.17	10.4	350	18.7/59.8

 This journal is © The Royal Society of Chemistry 2012

Published on 08 March 2012. Downloaded by UNIVERSITAT BAYREUTH on 9/4/2020 6:13:40 AM.

δ(N–Si–N) = 915 sh-875 *vs.* ^{1}H NMR ($CDCl_3$) (ppm): δ = 0.10 (br, SiCH_3), δ = 0.20 (vbr, SiCH_2CH$_2$B), δ = 0.78 (br, CH_3CHBSi), δ = 1.13 (br, SiCH$_2$CH_2B), δ = 1.21 (br, CH$_3$CHBSi), δ = 2.29 (vbr, NCH_3).

BmPS10.4 was obtained with a MA : TDSB ratio of 10.4 as a powder. Anal. found (wt%): C, 42.81; H, 11.89; N, 17.22; B, 3.57; Si, 24.17; O, 0.34 $[Si_{3.0}B_{1.1}C_{12.5}N_{4.3}H_{41.2}]_n$ ([348.04]$_n$). Calcd C, 46.25; H, 9.70; N, 13.54; B, 3.42; Si, 27.04 $[Si_{3.0}B_{1.0}C_{12.0}N_{3.0}H_{30.0}]_n$. IR (KBr/cm^{-1}): ν(N–H) = 3425, 3321, 3229 w; ν(C–H) = 2954 s, 2898 s, 2803 m; δ(N(H)CH$_3$) = 1600 w; δ_{asym}(CH$_3$) = 1463 w; ν(C–C) = 1355 w; δ(Si–CH$_3$) = 1254 s; δ(C–B–C) = 1187 m; δ(SiCH$_2$C) = 1139 m; ν(C–N) = 1061 m; δ(N–Si–N) = 914 sh-875 *vs.* ^{1}H NMR ($CDCl_3$) (ppm): δ = 0.10 (br, SiCH_3), δ = 0.22 (vbr, SiCH_2CH$_2$B), δ = 0.80 (br, CH_3CHBSi), δ = 1.10 (br, SiCH$_2$CH_2B), δ = 1.25 (br, CH$_3$CHBSi), δ = 2.32 (vbr, NCH_3).

2.4. Melt-spinning

Green fibers have been prepared by polymer melt-spinning in a nitrogen atmosphere using a lab-scale piston extrusion system (Matériau Ingéniérie-St-Christol les Alès, France). It enables definite throughputs and specific adjustment of fiber dimensions by properly adjusting the take-up velocity of the wind-up spool. Polymers **BmPS9.0 → BmPS10.4** (2.5 g) were molten by heating within a heater block until an appropriate viscosity was obtained and progressively compacted by a piston. The molten polymer flow was then driven through heated elements containing a filter and spinneret having a single 0.2 mm capillary. The resulting polymer emerging from the capillary at an ideal pressure of ~350 N as an endless filament was stretched and continuously collected on a rotating spool. The distance from the rotating spool to the spinneret was fixed at 13 cm. Extrusion and drawing units are designed for small scale spinning and can support flow throughputs from 0.1 mm min^{-1} to 2 mm min^{-1} and take-up velocity from 9 m min^{-1} to 330 m min^{-1}.

2.5. Curing and pyrolysis

Green fibers collected on the spool have been introduced in a horizontal tube furnace (Nabertherm type RS 80/500/11, Germany). The tube was pumped under vacuum and refilled with ammonia (99.995%). Subsequently, samples were subjected to a cycle of ramping of 0.5 °C min^{-1} to 200 °C, dwelling there for 1 h in flowing ammonia. Ammonia was switched off after 1 h at 200 °C and nitrogen was introduced in the furnace which was held for 1 h at 200 °C then heated to 1000 °C (1 °C min^{-1}), dwelling there for 2 h, and then cooling down to RT at 5 °C min^{-1} to convert the cured fibers into $Si_{3.0}B_{1.0}C_{5.0}N_{2.4}$ fibers. Constant flow (200 mL min^{-1}) of ammonia and nitrogen (200 mL min^{-1}) were passed through the tube.

3 Results and discussion

3.1. Molecular design of BmPSs with enhanced melt-spinning properties

In the multi-step process depicted in Fig. 2, we sequenced several synthetic strategies coupling molecular chemistry and chemistry of materials to design BmPSs of the type $[B(C_2H_4SiCH_3NCH_3)_3]_n$ that display enhanced melt-spinning properties in comparison to conventional BmPSs of the type $[B(C_2H_4SiRNH)_3]_n$ (R = H,[47] $(NH)_{0.5}$,[47] CH_3 (ref. 43 and 47)) which yield extensively crosslinked systems with poor processability. BmPSs of the type $[B(C_2H_4SiCH_3NCH_3)_3]_n$ lead to $Si_{3.0}B_{1.0}C_{5.0}N_{2.4}$ ceramic fibers after curing and pyrolysis.

During the BmPS synthesis, a maximum degree of transformation of Si–Cl groups into Si–NHCH$_3$ can be reached by reaction of TDSB with excess of MA. The resulting Si–NHCH$_3$ groups polycondense at RT to build up the polymer network according to the ideal synthesis pathway depicted in Fig. 3.

The BmPSs considered here are expected to be composed of cyclic silazane units [–Si–N–]$_n$ based on former studies[40,47] containing methyl-bonded silicon and nitrogen and bridged by BC$_3$ units.

Formally, every chlorine atom present in TDSB (6 atoms) is substituted by a NHCH$_3$ group. Subsequent condensation yields Si–N(CH$_3$)–Si units. Methylamine hydrochloride is formed from hydrogen chloride and MA. Aminolysis of TDSB therefore requires at least 9 eq. of MA referred to TDSB. However, we observed that a large excess of MA significantly influenced the melt-spinning behavior of the derived BmPSs. To investigate the influence of different MA : TDSB ratios (≥9), aminolysis of TDSB at 0 °C in THF was performed with MA : TDSB ratios = 9.0, 9.2, 9.7, and 10.4 giving four representative BmPSs of the type $[B(C_2H_4SiCH_3NCH_3)_3]_n$ (**BmPS9.0 → BmPS10.4**). Above a MA : TDSB ratio of 10.4, BmPSs are viscous and therefore inappropriate for melt-spinning.

In a first part of this study, we focused on the effect of different MA : TDSB ratios on the polymer chemistry and structure.

Elemental analysis data of samples **BmPS9.0 → BmPS10.4** (Table 2) prove that precursor synthesis *via* the monomer route occurs in the expected pathway since they agree reasonably well with the theoretical values.

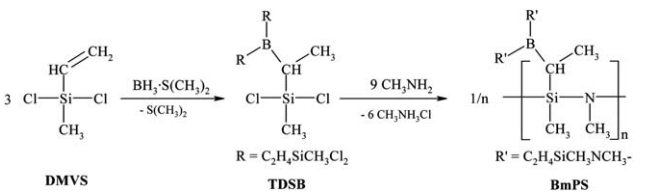

Fig. 3 Synthesis of BmPSs by aminolysis with methylamine (MA) of tris(dichloromethylsilylethyl)borane (TDSB, $B(C_2H_4SiCH_3Cl_2)_3$). Hydroboration is not regioselective and occurs at the α- and β-positions of the vinyl group (C_2H_4=$CHCH_3$, CH_2CH_2).

Table 2 Elemental composition of samples **BmPS9.0 → BmPS10.4**

BmPS	Empirical formula per monomer unit[a]
Calculated	$Si_{3.0}B_{1.0}C_{12.0}N_{3.0}H_{30.0}$
9.0	$Si_{3.0}B_{1.1}C_{11.3}N_{3.3}H_{36.8}$
9.2	$Si_{3.0}B_{1.1}C_{11.8}N_{3.6}H_{37.7}$
9.7	$Si_{3.0}B_{1.1}C_{12.2}N_{3.8}H_{39.6}$
10.4	$Si_{3.0}B_{1.1}C_{12.5}N_{4.3}H_{41.2}$

[a] Oxygen content ≤2 wt% and was therefore omitted in the calculation of the empirical formula.

Published on 08 March 2012. Downloaded by UNIVERSITAT BAYREUTH on 9/4/2020 6:13:40 AM.

In particular, the Si : B ratio of 3 : 1 in TDSB is more or less retained in the derived BmPSs (Si : B = 3 : 1.1). There is, in contrast, a deviation of the determined nitrogen, carbon and hydrogen values from those calculated. In particular, the proportion of carbon, nitrogen and hydrogen increases from sample **BmPS9.0** to sample **BmPS10.4** in relation with the increase in the MA : TDSB ratio. The found values for **BmPS9.7** and **BmPS10.4** are higher than expected and terminal $-N(H)CH_3$ groups are most likely the reason for excessive nitrogen. For excessive carbon contents, the presence of terminal carbon-based groups linked to silicon is suggested. The ideal chemical formulae of both **BmPS9.7** and **BmPS10.4** are $[Si_{3.0}B_{1.0}C_{12.0}N_{3.0}H_{30.0}]_n$ whereas the measured formulae are $[Si_{3.0}B_{1.1}C_{12.2}N_{3.8}H_{39.6}]_n$ and $[Si_{3.0}B_{1.1}C_{12.5}N_{4.3}H_{41.2}]_n$, respectively. Such compositions can be traced back to incomplete transamination of B $[C_2H_4Si(CH_3)(NHCH_3)_2]_3$ ($Si_{3.0}B_{1.0}C_{15.0}N_6H_{45.0}$) during addition of MA on TDSB.

Since a single TDSB molecule possesses 6 Si-bonded Cl atoms, 6 $N(H)CH_3$ units may be incorporated in the structure during aminolysis *via* a nucleophilic substitution. Condensation of MA forms two $Si–NHCH_3$ units that release $Si–N(CH_3)–Si$ moieties, thereby forming the polymeric framework. On the first view, the chemical formulae should be thus independent of the MA : TDSB ratio chosen during the synthesis. This suggests that there are other reactive sites. In order to determine the polymer structure in more detail, *i.e.*, to understand the influence of the MA : TDSB ratio on the structure, all samples **BmPS9.0** → **BmPS10.4** have been studied by ^{11}B, ^{13}C and ^{29}Si NMR. NMR spectroscopy is probably the most powerful tool to investigate the molecular structure of poly-silane, -carbosilane, -silazanes, -carbosilazanes, -borazylene, *etc.* and it is very frequently applied to investigate precursors of Si/C,[41] Si/C/N,[57,58] Si/B/C/N[18,59–62] and B/N[63] systems. Solid-state NMR studies (^{11}B, ^{13}C, ^{29}Si, and ^{15}N) have been shown to be extremely useful in the determination of even minor changes in the local environment during both the polymer synthesis and the polymer-to-ceramic conversion.

It should be emphasized that the two-step polymer synthesis typically gives rise to a large variety of structural components which are not all explicitly shown in the idealized chemical structure illustrated in Fig. 3. Here, we try to give a detailed picture of the structure of BmPSs of the type $[B(C_2H_4SiCH_3NCH_3)_3]_n$ (C_2H_4=$CHCH_3$, CH_2CH_2) based on the local silicon, boron and carbon environments. ^{11}B, ^{13}C and ^{29}Si are sufficiently abundant to be studied without isotopic enrichment. Nevertheless, ^{13}C spectra were recorded using the CP technique to obtain spectra with a reasonable signal-to-noise (*S*/*N*) ratio.

The experimental and simulated ^{13}C CP MAS NMR spectra of samples **BmPS9.0** → **BmPS10.4** are given in Fig. 4a. They exhibit three main signals centered at −3, 11 and 30 ppm which can be assigned on the basis of former studies on related compounds[18,59–63] and on the use of the Inversion Recovery Cross Polarization (IRCP) technique (Fig. 4b). In this type of experiments, the dynamics of polarization inversion depend on the proton environment.[64–66] As an illustration, the IRCP spectra of **BmPS9.0** (Fig. 4b) recorded at inversion times of 5 and 100 μs exhibit two signals inverting very rapidly at 5.7 and 16.7 ppm therefore assigned to $–CH_2–$ units. Based on its slower inversion, the signal at 11.2 ppm has been attributed to CH groups. First,

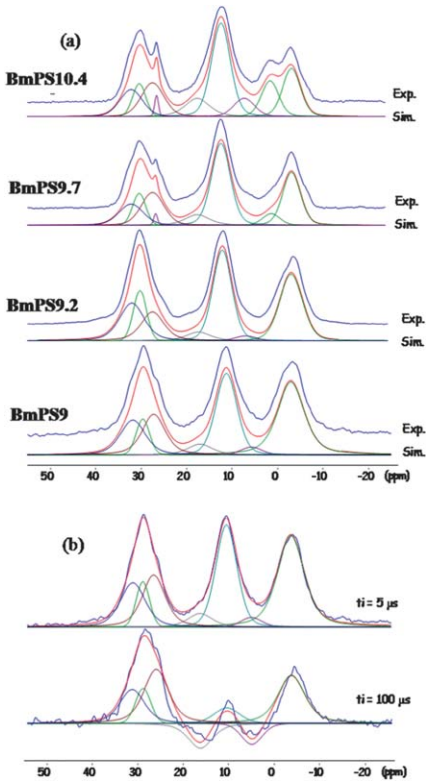

Fig. 4 Experimental and simulated (a) ^{13}C CP MAS spectra recorded for samples **BmPS9.0** → **BmPS10.4** and (b) ^{13}C IRCP MAS spectra of sample **BmPS9.0** recorded for inversion times t_i of 5 and 100 μs.

the results confirm the lack of regio-selectivity in the addition of borane dimethylsulfide to the Si–C=C units of DMVS during the synthesis of TDSB. Accordingly, resonances of both $–CH(CH_3)–$ and $–CH_2CH_2–$ units connecting Si and B in the native polymer appear in the ^{13}C NMR spectra. The other resonances at −2.8, 26.8, 29.6 and 31.0 ppm have still largely positive values for an inversion time of 100 μs. Since no quaternary carbon atoms are expected to be present, these signals have been assigned to CH_3 environments exhibiting a weak $^{13}C–^{1}H$ dipolar coupling due to their mobility.[67] As expected, NCH_3 (31 ppm) and $SiCH_3$ (−2.8 ppm) units are identified. The presence of terminal $–N(H)CH_3$ units is also confirmed through the appearance of the signal at 29.6 ppm. Unexpectedly, a narrow signal emerged in the $Si–CH_3$ region at 26.8 ppm in samples **BmPS9.7** and **BmPS10.4**. We suggested that it could be eventually assigned to terminal $–N(H)CH_3$ groups linked to boron.[63] Moreover, a distinct signal in the ^{13}C NMR spectrum of **BmPS10.4** is observed at a value typical for a Si-bonded methyl group region. A signal with the same chemical shift is present in smaller quantities in sample **BmPS9.7**. A signal with the same chemical shift is observed in the boron-modified polysilazanes containing NH functions,[62] *i.e.* in $Si(Me)(NH)_2$ units. According to the presence of $N(H)CH_3$ groups, we attributed this signal to Si-bonded methyl groups in which Si is bound to two $N(H)CH_3$ units, *i.e.*, $BC_2–Si(CH_3)–(N(H)CH_3)_2$.

Although the Cross-Polarisation (CP) response is not fully quantitative when comparing signals of units with various degrees of protonation, the comparison of intensities for a given

 This journal is © The Royal Society of Chemistry 2012

Published on 08 March 2012. Downloaded by UNIVERSITAT BAYREUTH on 9/4/2020 6:13:40 AM.

Table 3 ^{13}C CP MAS NMR characterization of samples **BmPS9.0** → **BmPS10.4**

	Proportion in BmPS (%)				
Position (δ)/ppm	**9.0**	**9.2**	**9.7**	**10.4**	Structural units
31	13	17	10	10	NCH_3
29.6	7	10	8	7	$N(H)CH_3$
26.8	16	12	16	13	Si–CH(*C*H$_3$)–B
26.1	—	—	1	1	CH_3NH_2
16.7	5	4	6	8	Si-CH_2*C*H$_2$-B
11.2	24	29	32	30	Si–*C*H(CH$_3$)–B
5.7	3	2	4	6	Si-*C*H$_2$CH$_2$-B
0.7	—	—	4	10	H$_3$*C*Si–NHCH$_3$
−2.8	32	26	19	15	$SiCH_3$

structural unit in the various polymers is a good indicator of the progress of the polymer synthesis. Table 3 reports the proportion of each structural unit calculated based on the intensities of signals assigned in the ^{13}C solid-state NMR spectra of **BmPS9.0** → **BmPS10.4**.

Results suggest an excess of $SiCH_3$ units relative to NCH_3 groups in the polymer structures, whereas a stoichiometry is expected. This is particularly the case for samples **BmPS9.7** and **BmPS10.4** that display a signal at 0.7 ppm assigned to $SiCH_3$ units linked to $N(H)CH_3$ groups which is not present in samples **BmPS9.0** and **BmPS9.2**. This confirms the excess of carbon contents measured by microanalysis especially on samples **BmPS9.7** and **BmPS10.4**.

^{29}Si and ^{11}B NMR spectra of **BmPS9.0** → **BmPS10.4** are displayed in Fig. 5 and 6, respectively.

All ^{29}Si NMR spectra exhibit a main broad line centered at 0 ppm assigned to Si atoms in a C_2N_2 environment which is in good agreement with the expected structure. This signal has a tendency to broaden with increasing the MA : TDSB ratio above 9.2 suggesting structural changes.

The ^{29}Si chemical shift depends on the conformation of the silazane.[62] For example, a ^{29}Si chemical shift value of −5 ppm is expected for SiC_2N_2 units within six-membered cyclosilazanes[68]

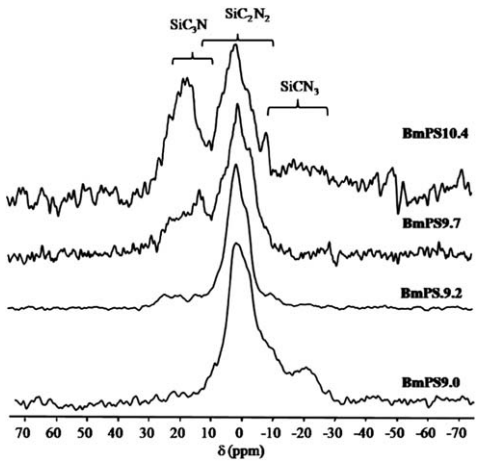

Fig. 5 Experimental ^{29}Si MAS NMR spectra recorded for samples **BmPS9.0** → **BmPS10.4** and chemical shift ranges expected for SiC_xN_{4-x} groups according to the literature.

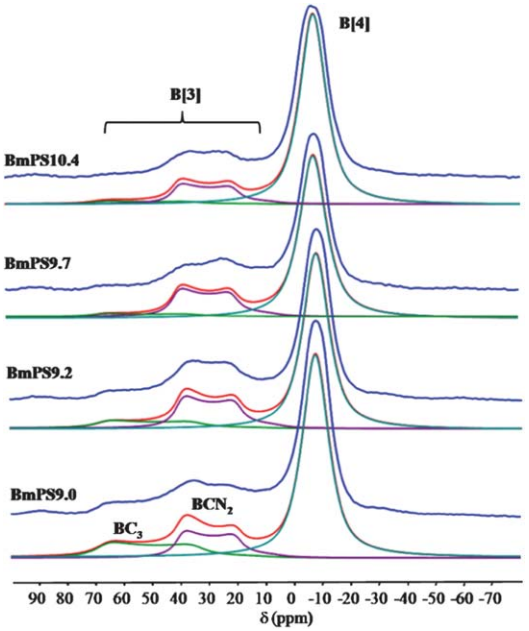

Fig. 6 Experimental and simulated ^{11}B MAS NMR spectra recorded for samples **BmPS9.0** → **BmPS10.4**.

while those of SiC_2N_2 groups in four- or eight-membered rings would appear at 3.3 ppm or −8.7 ppm, respectively.[68] Again, the resonance of linear SiC_2N_2 groups exhibits chemical shift values of *ca.* 2.2 ppm.[69] In conclusion, **BmPS9.0** → **BmPS9.2** are preferentially composed of four- and six-membered Si–N rings as well as Si–N chains, whereas there is no indication for the presence of eight-membered rings according to the position of the signal corresponding to an SiC_2N_2 environment centred at −2.1 ppm. In **BmPS9.7** and particularly in **BmPS10.4**, the signal broadens toward higher chemical shifts suggesting that four-membered rings and linear silazanes are best formed. In the spectra of sample **BmPS9**, an additional signal with a lower intensity is observed at higher field (−20 ppm) possibly attributed to some $SiCN_3$ units.

In **BmPS9.2** and more evident in **BmPS9.7** → **10.4**, spectra show a signal from 30 to 10 ppm assigned to SiC_3N units in agreement with the groups usually identified in BmPSs of the type $[B(C_2H_4SiRNH)_3]_n$ (R = H,[47,60] $(NH)_{0.5}$,[47] CH_3 (ref. 43,47,61 and 62)) and other polyborosilazanes[59] from the literature. This clearly indicates structural rearrangement during polymer synthesis according to eqn (1).

$$SiC_2N_2 + BC_3 \rightarrow SiC_3N + BC_2N \quad (1)$$

Experimental ^{11}B MAS NMR spectra recorded at 9.4 T are shown in Fig. 6. They exhibit broadened and overlapping signals in the range of 70 to 10 ppm and well-defined resonance around −10 ppm.

^{11}B is a quadrupolar nucleus ($I = 3/2$). As a consequence, the isotropic chemical shift value for such a nucleus does not correspond to the barycentre of the resonance signal, which is dominated by the second-order quadrupolar broadening.[70] According to the proposed structure of the polymer (see Fig. 3), the presence of BC_3-coordination environments, *i.e.*, tri-coordinated boron, is expected. However, the experimental spectra

Published on 08 March 2012. Downloaded by UNIVERSITAT BAYREUTH on 9/4/2020 6:13:40 AM.

reflect a large heterogeneity in the local chemical environment of the boron nuclei: both distorted tetrahedral and trigonal coordinations are identified. This is a common structural feature observed in BmPSs.[62] The narrow signal centered at −10 ppm suggests the presence of distorted tetra-coordinated boron sites[62] while two main signals with δ_{iso}(^{11}B) at 76.5 and 45.8 ppm and C_Q values of 4 and 3.3 MHz respectively are necessary to simulate the tri-coordination. Based on the chemical shift values, the tri-coordinated boron can be assigned to BC_3 and BCN_2 environments respectively.[62] However, the presence of BC_2N units cannot be excluded as suggested in eqn (1). Here, we cannot distinguish such units according to the high proportion of tetra-coordinated boron. It should be mentioned that a precise determination of the exact nature of tetra-coordinated boron neighbors is not possible. However, the position suggests that boron is not protonated, and considering the synthesis and previous NMR observations, the formation of $BC_{4-x}N_x$ entities is reasonable. Tetrahedral coordination of boron is more present in boron-modified polysilazanes obtained by aminolysis (reaction with MA) compared to those obtained by ammonolysis[62] (reaction with ammonia). Furthermore, it can be noticed that their proportion in comparison to tri-coordinated boron increases from **BmPS9.0** to **BmPS10.4** as indicated in Table 4.

This can be linked to the fact that MA is a stronger Lewis base than ammonia. TDSB has two Lewis acidic centers: boron (BC_3) and silicon (C_2SiCl_2) atoms. Due its higher basicity compared with NH_3, MA is less selective and may therefore attack both boron and silicon atoms of TDSB. It is even remarkable that the portion of BC_3 groups is particularly low in sample **BmPS10.4** which means that the structure of **BmPS10.4** is far from that idealized in Fig. 3 in which only BC_3 units are expected.

By combining multinuclear (^{13}C, ^{29}Si, and ^{11}B) solid-state NMR data with results derived from elemental analyses, it is clear that the real structure of BmPSs of the type $[B(C_2H_4SiCH_3NCH_3)_3]_n$ (C_2H_4=$CHCH_3$, CH_2CH_2) differs from the ideal structure suggested in Fig. 3. Fig. 7 reports the structural units which have been identified by ^{13}C, ^{29}Si and ^{11}B solid-state NMR and common to all samples. It should be mentioned that $SiCN_3$ and SiC_3N units which are not common to all samples have not been illustrated in Fig. 7.

At this step of the study, we can only admit that an increasing MA : TDSB ratio increases the portion of terminal $N(H)CH_3$ groups. The N atoms in the latter are sterically less shielded than those with chains or rings, *i.e.*, [–Si–N]. Moreover, BmPSs with MA : TDSB > 9.2 seem to be composed in part of linear silazane features with a reduced chain entanglement. Since physical–chemical properties which are important for melt-spinning are directly connected to the structure of the polymer, the synthesis conditions, *i.e.*, the MA : TDSB ratio, will affect the melt-spinnability of BmPSs. It is therefore mandatory to give a general view of the polymer structure as a function of the MA : TDSB ratio which should be supported by molecular weight measurements of samples **BmPS9.0** → **BmPS10.4**.

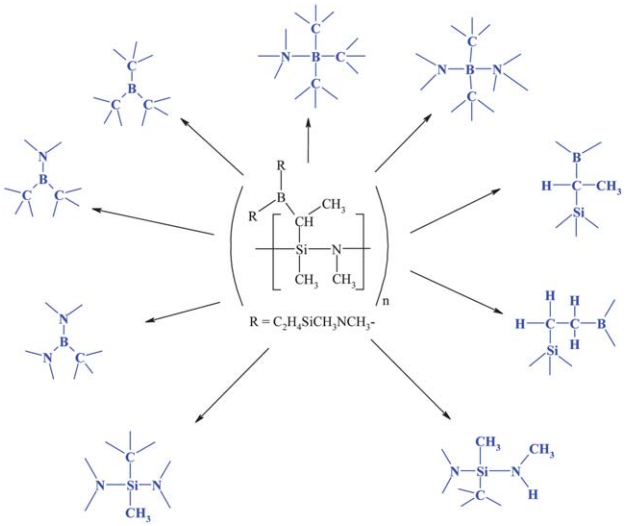

Fig. 7 Structural units identified by ^{13}C, ^{29}Si and ^{11}B in a typical BmPS $[B(C_2H_4SiCH_3NCH_3)_3]_n$ (C_2H_4=$CHCH_3$, CH_2CH_2).

3.2. Glass transitions and molecular weight measurements

BmPS9 → **BmPS10.4**, which are solid at RT, are transformed into viscous materials by passing through glass transitions at relatively low temperature (T_g). The low value of T_g probably results from the low cross-linking density of the polymer network. From Table 5, it can be concluded that T_g decreases with increasing MA : TDSB ratio from **BmPS9.0** (T_g = 51 °C) to **BmPS10.4** (T_g = 32 °C).

Gel Permeation Chromatography with polystyrene standards and THF as the mobile phase has been performed in order to observe the effect of the MA : TDSB ratio on the molecular weight of the corresponding BmPSs as well as the relationship between T_g and M_w. Data tend to demonstrate that the molecular weight decreases from **BmPS9.0** (706.7 g mol^{-1}) to **BmPS10.4** (248.7 g mol^{-1}) with a polydispersity index (PDI) changing independently of the MA : TDSB ratio (Table 5). **BmPS9.0** and **BmPS9.2** have molecular weights which correspond to $n \approx 2.5$. In contrast, BmPSs with MA : TDSB ratio >9.2 have lower molecular weights. The respective value of **BmPS10.4** is even below that of the monomeric unit (311.45 g mol^{-1}). The molecular weight of a BmPS having a MA : TDSB

Table 4 ^{11}B MAS NMR characterization of samples **BmPS9.0** → **BmPS10.4**

			Proportion in BmPS (%)				
δ_{iso}/ppm	C_Q/MHz	η	**9.0**	**9.2**	**9.7**	**10.4**	Assignment
76.5	4.2	0	13	8	6	4	BC_3
45.8	3.3	0	17	22	19	15	BCN_2
−7.6	—	—	70	70	75	79	$BC_{4-x}N_x$

Table 5 Molecular weight measurements and polydispersity degrees for samples **BmPS9.0** → **BmPS10.4**

BmPS	T_g/°C	Molecular number/ g mol^{-1}	Molecular weight/ g mol^{-1}	PDI
9.0	51	277.1	706.7	2.55
9.2	43	378.6	631.5	1.67
9.7	37	228.3	549.9	2.41
10.4	32	187.5	248.7	1.33

 This journal is © The Royal Society of Chemistry 2012

Published on 08 March 2012. Downloaded by UNIVERSITAT BAYREUTH on 9/4/2020 6:13:40 AM.

ratio of 10.6 (**BmPS10.6**, 216.2 g mol^{-1}) confirms the tendency of the molecular weight of BmPSs to decrease with the increase of the MA : TDSB ratio. In comparison, Riedel *et al.* measured an average molecular weight M_w = 1099 g mol^{-1} corresponding to n = 3–5 and a polydispersity of 1.28 for $[B(C_2H_4SiCH_3NH)_3]_n$ (C_2H_4=$CHCH_3$, CH_2CH_2) prepared by ammonolysis of TDSB with 9 eq. of NH_3.[47] This clearly indicated that initially formed $N(H)CH_3$ units have a lower ability to self-condense during the formation of $[B(C_2H_4SiCH_3NCH_3)_3]_n$ in comparison with initially formed NH_2 groups in the synthesis of $[B(C_2H_4CH_3RNH)_3]_n$.

In a first approximation, we can suggest that the evolution profile of T_g for **BmPS9.0 → BmPS10.4** follows a usual trend observed for conventional organic polymers which obey the Flory–Fox law: T_g linearly decreases with decreasing average values of the molecular weight (M_w) up to a certain value at which any changes in T_g are detected.[71,72] Upon addition of MA, replacement of the Cl atoms with $N(H)CH_3$ units and subsequent condensation take place to form the BmPS framework displaying a backbone structure of silicon and nitrogen atoms, alternating in occurrence. The backbone of silazanes of the type $[SiR_2NH]_n$ (R = H, CH_3, CH=CH_2) is known to form D3 (six-membered cyclosilazanes) and D4 (eight-membered cyclosilazanes)-type rings.[73]

Here, according to ^{29}Si solid-state NMR, molecular weight values and the lower reactivity of $N(H)CH_3$ in comparison to NH_2 groups, it is most probable that the rings are composed of four- and/or six-membered rings cross-linked *via* boron-based units including $BC_{3-x}N_x$ ($0 \leq x < 3$) and $BC_{4-x}N_x$ ($0 \leq x < 4$) and terminated by $N(H)CH_3$ groups as suggested by solid-state NMR results. This configuration is representative of BmPSs with MA : TDSB ratios of 9.0–9.2. Above a certain MA : TDSB ratio (most probably 9.2), terminating $N(H)CH_3$ groups are more abundant and as a consequence, the portion of $BC_{4-x}N_x$ ($0 \leq x \leq 4$) increases. As a conclusion, we can postulate that excess of MA leads to an incomplete transamination of the compound formed after substitution of chlorine atoms ($B[C_2H_4Si(CH_3)(NHCH_3)_2]_3$ ($Si_{3.0}B_{1.0}C_{15.0}N_6H_{45.0}$)), thereby leading to the formation of shorter, linear silazane chains with modification of the boron environment.

Based on this assumption, T_g values of samples **BmPS9.0 → BmPS10.4** can be clearly understood: The decrease in T_g is a consequence of the chain disentanglement according to the formation of terminal groups such as $N(H)CH_3$ groups and an increasing portion of tetra-coordinated boron. The end-groups promoted mobility to the BmPS chains similar to plasticizers in classical organic polymers. As a result, the BmPSs possess improved spinning behavior.

3.3. Melt-spinnability of BmPSs

The possibility of adjusting the chemical composition, structural configuration and physical–chemical properties of BmPSs through modification of the molecular parameters is a key point in optimizing their melt-spinning. Herein, we investigated the spinning behaviour of samples **BmPS9.0 → BmPS10.4** through CCD camera visualization of fiber geometry during extrusion and fiber stretching. The studies were based on two objectives to reach: (1) stability of the melt during the spinning process and (2) extrusion with capillary stability upon stretching.

The melt-spinnability of the polymer can be defined as its ability to be extruded at a certain temperature, and then stretched as an endless fiber without being damaged or broken. First orienting investigations of the stretchability of polymer fibers derived from samples **BmPS9.0 → BmPS10.4** were performed by pulling the related melt, which fell with gravity, manually to a distance of 5–30 cm. It was observed that the best stretching was measured 13 cm below the exit of the capillary which had a diameter of 200 μm. Therefore, the wind-up spool was placed 13 cm below the exit of the capillary. Melt-spinning was then conducted with the same throughput, with an increasing take-up velocity until the spinning line failed, determining the limit of spinnability, thereby the maximum drawdown ratio being defined as the take-up velocity-to-extrusion velocity ratio. Spinning was monitored using a high-resolution camera put inside the glove-box, and oriented towards the fiber at the exit of the capillary.

Values of the spinning temperatures (T_S), extrusion velocities (V_E), take-up velocities (V_T), and drawdown ratios defined as V_T/V_E[74] are compiled in Table 6. Together, these variables control the green fiber diameter at the macroscopic level.

All BmPSs described here are spinnable at temperatures decreasing from 115 °C (**BmPS9.0**) to 93 °C (**BmPS10.4**). This is in good agreement with the decreasing T_g values from 51 °C to 32 °C with increasing MA : TDSB ratio. It is important to note that melt-spinning should occur in a temperature range in which no or only negligible decomposition occurs. (See the corresponding curve for **BmPS9.0** in the ESI (Fig. S1†).) **BmPS9.0**, for example, exhibits an appreciable thermal stability up to ~80 °C in flowing nitrogen. At this temperature, the weight loss rate is only ~0.2% min^{-1} and the weight loss itself is smaller (0.3%) if using a heating rate of 1 °C min^{-1}. If isothermally held at the spinning temperature, the decomposition rate will of course further decrease. The weight loss for each sample at T_s determined by TGA is reported in Table 6. Although decomposition occurs during spinning of polymers to a minor degree, the melt-spinnability is not affected and capillary instability in relation with polymer decomposition is clearly not observed. Fine-diameter green fibers can even be obtained for samples **BmPS9.0–BmPS9.2**. The stretchability of **BmPS9.7** and **BmPS10.4** are similar but lower than samples **BmPS9.0–BmPS9.2**. However, it should be mentioned that the values cannot be measured with accuracy because stretching occurred from a polymer drop as observed with the CCD camera during melt-spinning (Fig. 8 and 9). We can clearly distinguish two categories of responses to melt throughput and fiber stretching.

Fig. 8 shows pictures of the **BmPS9.0**-derived filament emerging from the die (a) and stretched by the spool (b and c). The as-extruded molten filament falls with gravity from the die (a) to be subsequently stretched from the melt at 115 °C without fiber breaking at a maximum drawdown ratio of 102.6. The melt flow remains stable during the spinning operation (30 min), thus leading to the reproducible preparation of green fibers with optimum quality in terms of surface appearance and uniform diameter ($d \approx$ 19.7 μm, Fig. 2). Such uniform and small diameters are required to obtain preferably thin ceramic fibers which possess high tensile strength after pyrolysis.

Published on 08 March 2012. Downloaded by UNIVERSITAT BAYREUTH on 9/4/2020 6:13:40 AM.

Table 6 Spinning parameters of samples **BmPS9.0** → **BmPS10.4**

BmPS	T_S[a] (± 1)/(°C)	V_E[b]/m s^{-1}	V_T[c]/m s^{-1}	Drawdown ratios κ[d]	Calculated fiber diameter d_f[e]/μm	Measured weight loss at T_s (wt%)[f]
9.0	115	0.038	3.9	102.6	19.7	−2.5
9.2	99	0.038	2.6	68.4	24.2	−2.7
9.7	97	0.038	1.5	39.5[g]	31.8	−1.7
10.4	93	0.038	2.1	55.3[g]	26.9	−1.8

[a] As measured by the thermocouples inside the chamber furnace. [b] Calculated from the piston velocity *via* volume displacement at a pressure of about 350 N. [c] Maximum measured velocity. [d] Defined as the drawdown ratio, $k = V_T/V_E$, see ref. 74. [e] Fibers ≈ $d_{Capillary} \times [(V_{Extrusion}/V_{Take\text{-}up})]1/2$. [f] Measured by TGA in flowing nitrogen (5 °C min^{-1}). [g] Overestimated because the fiber was formed by stretching the polymer drop.

BmPS9.7 and **BmPS10.4** flow very easily through the capillary at 97 °C and 93 °C. The polymer emerges as a molten drop at the exit of the capillary for both polymers (Fig. 9a) demonstrating the too low viscosity of such polymers. A relatively high extrusion velocity has to be applied to adjust an ideal spinning pressure (*i.e.*, 350 N) leading to extrusion instabilities during the stretching of the polymer and in the worst case breakage or non-reproducible diameters (Fig. 2).

Based on the structural features identified for the different BmPS samples (Fig. 7), we speculate that **BmPS9.0** and **BmPS9.2** display an appropriate chain entanglement with an adequate portion of plasticizing groups such as $N(H)CH_3$ units to be extruded then stretched into fine-diameter fibers. At the opposite, the low molecular weight of **BmPS10.4** renders the chain highly mobile providing an unsatisfactory viscosity, even at low temperatures. This fact could favor pure extrusion but the low molecular weight is an invincible barrier for the production of continuous fibers of sufficient quality: extrusion instability during the fiber stretching is observed and fiber breaking occurs (Fig. 2).

In good agreement with structural investigations, the control of molecular parameters such as the MA : TDSB ratio is therefore a crucial aspect for the spinning quality of BmPSs. Those prepared with a MA : TDSB ratio which does not exceed 9.2 (samples **BmPS9.0** and **BmPS9.2**) are readily spinnable, and fine-diameter fibers (~19.7 μm, Table 6) can be continuously produced and collected on a rotating spool by stretching the filament emerging from the spinneret at a relatively high spool velocity without capillary instability.

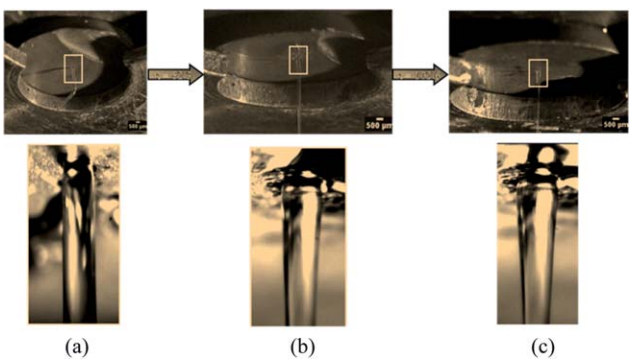

Fig. 8 CCD photos of extrusion (a) and stretching at various drawdown ratios (b and c) of sample **BmPS9.0**.

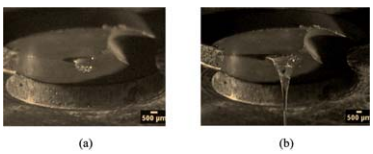

Fig. 9 CCD photos of capillary instability (a) and upon stretching (b) of sample **BmPS9.7**.

3.4. Thermal decomposition of the green fibers

The MA : TDSB ratio has no significant effect on the value of the ceramic yields which were determined by TGA up to 1000 °C in flowing nitrogen. Respective data are provided in Table 7.

Most probably, the ceramic yield is predominantly affected by the volatilization of low molecular weight species during the BmPS-to-Si/B/C/N conversion independently of the MA : TDSB ratio. Remarkably, the integrity of green fibers is not preserved during the heat-treatment. Adopting a curing process under ammonia at 200 °C (dwelling time of 2 h) prior decomposition under nitrogen at 1000 °C is thus required to increase the ceramic yield while preserving the fiber cohesion.[36]

TGA values and ceramic yield depend on the macroscopic appearance of polymers (fibers or bulk). As an illustration, we compared the TG profiles of the as-synthesized **BMPS9.0** and green fibers obtained from **BmPS9.0** (Fig. 10).

Table 7 Ceramic yield measured by TGA under nitrogen at 1000 °C for samples **BmPS9.0** → **BmPS10.4**

BmPS	Ceramic yield
9.0	14.1
9.2	10.5
9.7	15.3
10.4	13.7

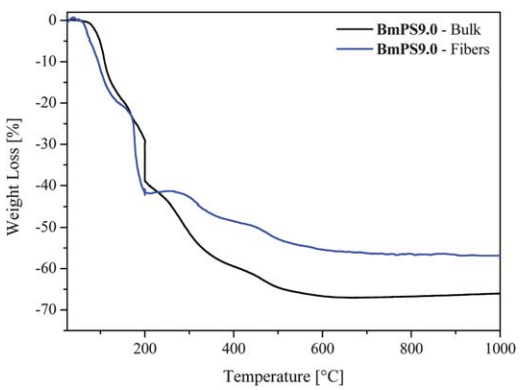

Fig. 10 TGA curves of **BmPS9.0**: bulk and fibers.

This journal is © The Royal Society of Chemistry 2012

Published on 08 March 2012. Downloaded by UNIVERSITAT BAYREUTH on 9/4/2020 6:13:40 AM.

It is observed that the profiles of the TG curves up to 200 °C are almost similar during the curing process. Degradation of the cured fibers proceeds more slowly and the ceramic yield is calculated to be 44 wt%. In contrast, cured powders release ceramics in *ca.* 33% yield. The weight loss associated with the polymer-to-ceramic conversion is usually governed by a complex interplay of several diffusion-type transport mechanisms which are nearly independent of the applied heating schedule.[23] We therefore suggested that the lower surface : volume ratio ($S : V$) of the fibers leads to a better NH_3 curing and therefore to a higher ceramic yield.

3.5. Mechanical properties and microstructure of $Si_{3.0}B_{1.0}C_{5.0}N_{2.4}$ ceramic fibers

To gather microstructural information about the fibers, TEM investigations were performed. Therefore, **BmPS9.0**-derived ceramic fibers have been investigated by high-resolution TEM coupled with the corresponding selected area electron diffraction (SAED) pattern (Fig. 11).

The SAED pattern displays diffuse and poorly discernible haloes indicating the presence of an amorphous microstructure. HRTEM investigation confirms that the selected specimen is featureless with an homogeneous microstructure. $Si_{3.0}B_{1.0}C_{5.0}N_{2.4}$ fibers prepared at 1000 °C are thus predominantly amorphous. The average diameter of the fibers measures 12.1 μm. They showed a room-temperature Weibull tensile strength of 1.4 GPa (for a failure probability of 0.63) and an average Young's modulus of 120 GPa (Fig. 12) according to the Weibull statistic. The low value of the Young's modulus can be a consequence of the amorphous state of the material.

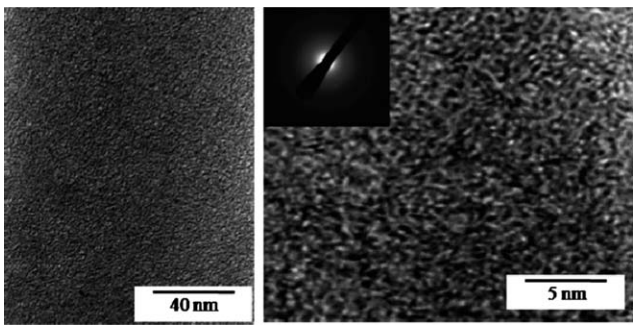

Fig. 11 HRTEM image showing the microstructure of **BmPS9.0**-derived $Si_{3.0}B_{1.0}C_{5.0}N_{2.4}$ fibers after pyrolysis to 1000 °C.

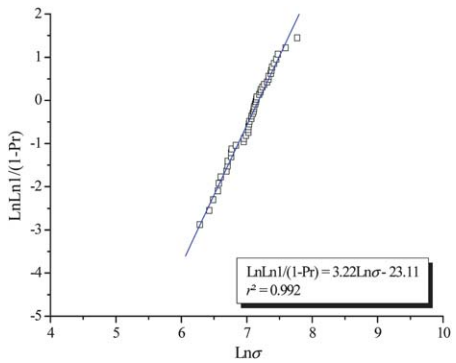

Fig. 12 Weibull plot of as-prepared $Si_{3.0}B_{1.0}C_{5.0}N_{2.4}$ fibers.

4 Conclusions

The role of the structure and chemistry of boron modified polysilazanes (BmPSs) of type $[B(C_2H_4SiCH_3NCH_3)_3]_n$ (C_2H_4= $CHCH_3$, CH_2CH_2) on their spinning behavior is discussed in this study using a series of four representative polymers. Particular attention has been given to the introduction of the appropriate amount of methylamine (MA) used during aminolysis of the trisdichlorosilylethylborane (TDSB). A MA : TDSB ratio in the range 9–9.2 allows generating polymers capable of producing green fibers in a stable process. They represent a complex polymeric network bridged *via* tri-coordinated $BC_{3-x}N_x$ units and tetra-coordinated BC_xN_{4-x} units connecting four and/or six-membered –Si–N– rings. The latter are terminated by $–N(H)CH_3$ groups. Such BmPSs display a chemical formula of $[Si_{3.0}B_{1.1}C_{11.35\pm0.5}N_{3.8\pm0.4}H_{8.15\pm1.35}]_n$ ($n = \sim2.5$), a glass transition at 48 ± 4 °C, tailored flexibility and sufficient plasticity to successfully produce fine-diameter green fibers at 107 ± 8 °C in a stable melt-spinning process. After melt-spinning, green fibers derived from **BmPS9.0** have been cured, then pyrolyzed up to 1000 °C to generate silicoboron carbonitride ($Si_{3.0}B_{1.0}C_{5.0}N_{2.4}$) fibers of 10–13 μm diameters according to an established procedure. Their thermal decomposition has been investigated and the fiber decomposition profile as well as the ceramic yield differed from those recorded for the same preceramic polymer in form of powders. Polymer fibers exhibit a ceramic yield of 44% after thermal decomposition at 1000 °C under nitrogen. The derived ceramic fibers exhibit a dense texture with a glassy section, indicating an amorphous state of the ceramic which was further confirmed by TEM as well as Weibull strengths of 1.4 GPa and Young's modulus of 120 GPa.

Acknowledgements

The authors gratefully acknowledge supporting co-workers at the LMI in Lyon and Prof. Arnaud Brioude for his contribution to TEM. We thank the European Community who supported this work through the Marie Curie Research Training Network PolyCerNet (Contract MRTN-CT-2005-019601).

Notes and references

1 P. G. Chantrell and E. P. Popper, in *Special Ceramics—4*, ed. E. P. Popper, Academic Press, New York, 1964, p. 87.
2 S. Yajima, J. Hayashi, M. Omori and K. Okamura, *Nature*, 1976, **261**, 683.
3 G. Winter, W. Verbeek and M. Mansmann, *US Pat.*, 3892583, 1975.
4 M. Peuckert, T. Vaahs and M. Brück, *Adv. Mater.*, 1990, **2**, 398.
5 J. Bill and F. Aldinger, *Adv. Mater.*, 1995, **7**, 775.
6 R. Riedel, G. Mera, R. Hauser and A. Klonczynski, *J. Ceram. Soc. Jpn.*, 2006, **114**, 425.
7 A. Staubitz, A. Presa Soto and I. Manners, *Angew. Chem.*, 2008, **120**, 6308.
8 M. Bechelany, S. Bernard, A. Brioude, P. Stadelmann, C. Charcosset, K. Fiaty, D. Cornu and P. Miele, *J. Phys. Chem. C*, 2007, **111**, 13378.
9 *Polymer Derived Ceramics: Theory and Applications*, ed. P. Colombo, G. D. Soraru, R. Riedel and A. Kleebe, DEStech Publications, Inc., 2009.
10 P. Colombo, G. Mera, R. Riedel and G. D. Soraru, *J. Am. Ceram. Soc.*, 2010, **93**, 1805.
11 J. Kong, T. Schmalz, G. Motz and A. H. E. Müller, *Macromolecules*, 2011, **44**, 1280.
12 (*a*) E. Kockrick, P. Krawiec, U. Petasch, H.-P. Martin, M. Herrmann and S. Kaskel, *Chem. Mater.*, 2008, **20**, 77–83; (*b*) E. Kockrick,

Published on 08 March 2012. Downloaded by UNIVERSITAT BAYREUTH on 9/4/2020 6:13:40 AM.

R. Frind, M. Rose, U. Petasch, W. Böhlmann, D. Geiger, M. Herrmann and S. Kaskel, *J. Mater. Chem.*, 2009, **19**, 1543.
13 C. Vakifahmetoglu, I. Menapace, A. Hirsch, L. Biasetto, R. Hauser, R. Riedel and P. Colombo, *Ceram. Int.*, 2009, **35**, 3281.
14 (*a*) H. Wang, S. Y. Zheng, X. D. Li and D. P. Kim, *Microporous Mesoporous Mater.*, 2005, **80**, 357; (*b*) J. Yan, A. Wang and D. P. Kim, *Microporous Mesoporous Mater.*, 2007, **100**, 128; (*c*) I. K. Sung, Christian, M. Mitchell, D. P. Kim and P. J. A. Kenis, *Adv. Funct. Mater.*, 2005, **15**, 1336.
15 (*a*) J. Wan, A. Alizadeh, S. T. Taylor, P. R. L. Malenfant, M. Manoharan and S. M. Loureiro, *Chem. Mater.*, 2005, **17**, 5613; (*b*) P. R. L. Malenfant, J. Wan, S. T. Taylor and M. Manoharan, *Nat. Nanotechnol.*, 2007, **2**, 43.
16 Q. D. Nghiem, D. P. Kim and S. O. Kim, *J. Nanosci. Nanotechnol.*, 2008, **8**, 5527.
17 X. B. Yan, P. Dibandjo, S. Bernard, L. Gottardo, H. Mouttaabidd and P. Miele, *Chem. Mater.*, 2008, **20**, 6325.
18 O. Majoulet, J. G. Alauzun, L. Gottardo, C. Gervais, M. E. Schuster, S. Bernard and P. Miele, *Microporous Mesoporous Mater.*, 2011, **140**, 40.
19 H. Wang, J. S. Yu, X. D. Li and D. P. Kim, *Chem. Commun.*, 2004, 2352.
20 U. Kusari, Z. Bao, Y. Cai, G. Ahmad, K. H. Sandhage and L. G. Sneddon, *Chem. Commun.*, 2007, 1177.
21 M. M. Guron, X. Wei, D. Welna, N. Krogman, M. J. Kim, H. Allcock and L. G. Sneddon, *Chem. Mater.*, 2009, **21**, 1708.
22 V. Salles, S. Bernard, A. Brioude, D. Cornu and P. Miele, *Nanoscale*, 2010, **2**, 215.
23 S. Bernard, K. Fiaty, D. Cornu, P. Miele and P. Laurent, *J. Phys. Chem. B*, 2006, **110**, 9048.
24 M. Günthner, T. Kraus, A. Dierdorf, D. Decker, W. Krenkel and G. Motz, *J. Eur. Ceram. Soc.*, 2009, **29**, 2061.
25 J. Li, V. Salles, S. Bernard, C. Gervais and P. Miele, *Chem. Mater.*, 2010, **22**, 2010.
26 T. A. Pham, D. P. Kim, T.-W. Lim, S. H. Park, D. Y. Yang and K. S. Lee, *Adv. Funct. Mater.*, 2006, **16**, 1235.
27 (*a*) S. H. Lee and M. Weinmann, *Acta Mater.*, 2009, **57**, 4374; (*b*) S. H. Lee, M. Weinmann, P. Gerstel and F. Aldinger, *Scr. Mater.*, 2008, **59**, 607.
28 L. A. Liew, R. A. Saravanan, V. M. Bright, M. L. Dunn, J. W. Daily and R. Raj, *Sens. Actuators, A*, 2003, **103**, 171.
29 A. Asthana, K. O. Kim, J. Perumal, D.-M. Kim and D. P. Kim, *Lab Chip*, 2009, **9**, 1138.
30 (*a*) G. E. Legrow, T. F. Lim, J. Lipowitz and R. S. Reaoch, *Am. Ceram. Soc. Bull.*, 1987, **66**, 363; (*b*) J. Lipowitz, *Fiber Synthesis Processes, in Carbide, Nitride and boride Materials, Synthesis and Processing*, ed. A. W. Weimer, Chapman and Hall, London, 1997, p. 433; (*c*) J. Lipowitz, J. A. Rabe, A. Zangvil and Y. Xu, *Ceram. Eng. Sci. Proc.*, 1997, **18**, 147.
31 R. Bunsell and M.-H. Berger, in *Fine Ceramic Fibres*, Marcel Dekker ed., Inc., NY, 1999.
32 G. Motz, J. Hacker, G. Ziegler, B. Clauss and D. Schawaller, Low-Cost-Ceramic SiCN Fibers By an Optimized Polycarbosilazane and Continuous Processing, in *Inorganic Structural Fiber Composites*, ed. P. Vincenzini and C. Badini, 2003, p. 47.
33 H. P. Baldus, M. Jansen and D. Sporn, *Science*, 1999, **285**, 699.
34 P. Miele, S. Bernard, D. Cornu and B. Toury, *Soft Matter*, 2006, **4**, 249.
35 J. A. DiCarlo and H. M. Yun, Non-Oxide (Silicon Carbide) Fibers, in *Handbook of Ceramic Composites*, ed. N. P. Bansal, New York, Kluwer Academic Publishers, 2005, p. 33.
36 (*a*) S. Bernard, M. Weinmann, D. Cornu, P. Miele and F. Aldinger, *J. Eur. Ceram. Soc.*, 2005, **25**, 251; (*b*) S. Bernard, M. Weinmann, P. Gerstel, P. Miele and F. Aldinger, *J. Mater. Chem.*, 2005, **15**, 289.
37 T. Ishikawa, Y. Kohtoku, K. Kumagawa, T. Yamamura and T. Nagasawa, *Nature*, 1998, **391**, 773.
38 Z. Xie, S. Cao, J. Wang, X. B. Yan, S. Bernard and P. Miele, *Mater. Sci. Eng., A*, 2010, **527**, 7086.
39 R. M. Laine and A. Sellinger, *Si-Containing Ceramic Precursors in the Chemistry of Organic Silicon Compounds*, ed. S. Patai and Z. Rappoport, John Wiley & Sons, New York, 1998, vol. 2, ch. 39, p. 2245.
40 E. Kroke, Y. L. Li, C. Konetschny, E. Lecomte, C. Fasel and R. Riedel, *Mater. Sci. Eng., R*, 2000, **26**, 97.
41 R. M. Laine and F. Babonneau, *Chem. Mater.*, 1993, **5**, 60.
42 S. Bernard, S. Duperrier, D. Cornu, P. Miele, M. Weinmann, C. Balan and F. Aldinger, *J. Optoelectron. Adv. Mater.*, 2006, **8**, 648.
43 M. Weinmann, J. Schuhmacher, H. Kummer, S. Prinz, J. Peng, H. J. Seifert, M. Christ, K. Müller, J. Bill and F. Aldinger, *Chem. Mater.*, 2000, **12**, 623.
44 (*a*) S. Duperrier, C. Gervais, S. Bernard, D. Cornu, F. Babonneau, C. Balan and P. Miele, *Macromolecules*, 2007, **40**, 1018; (*b*) S. Duperrier, S. Bernard, A. Calin, C. Sigala, R. Chiriac, P. Miele and C. Balan, *Macromolecules*, 2007, **40**, 1028.
45 P. Toutois, P. Miele, S. Jacques, D. Cornu and S. Bernard, *J. Am. Ceram. Soc.*, 2006, **89**, 42.
46 (*a*) H. P. Baldus, O. Wagner and M. Jansen, *MRS Online Proc. LIbr.*, 1992, **271**, 821; (*b*) H. P. Baldus, M. Jansen and O. Wagner, *Key Eng. Mater.*, 1994, **89-91**, 75; (*c*) H. P. Baldus and M. Jansen, *Angew. Chem.*, 1997, **109**, 338; (*d*) H. P. Baldus, A. Thierauf, R. Henborn and D. Sporn, *US Pat.*, 5885519, 1999.
47 R. Riedel, A. Kienzle, W. Dressler, L. Ruwisch, J. Bill and F. Aldinger, *Nature*, 1996, **382**, 796.
48 M. Weinmann, T. W. Kamphowe, J. Schuhmacher, K. Müller and F. Aldinger, *Chem. Mater.*, 2000, **12**, 2112.
49 M. Takamizawa, T. Kobayashi, A. Hayashida and Y. Takeda, *US Pat.*, 4604367, 1986.
50 (*a*) L. Lu, C. X. Feng and Y. C. Song, *J. Mater. Sci. Lett.*, 1998, **17**, 481; (*b*) L. Lu, C. X. Feng and Y. C. Song, *J. Mater. Sci. Lett.*, 1998, **17**, 599; (*c*) Z. Y. Chu, C. X. Feng and Y. C. Song, *J. Mater. Sci. Lett.*, 2003, **22**, 725.
51 (*a*) T. Wideman, E. Cortez, E. E. Remsen, G. A. Zank, P. J. Carroll and L. G. Sneddon, *Chem. Mater.*, 1997, **9**, 2218; (*b*) T. Wideman, P. J. Fazen, K. Su, E. E. Remsen, G. A. Zank and L. G. Sneddon, *Appl. Organomet. Chem.*, 1998, **12**, 681.
52 M. K. Cinibulk and T. A. Parthasarathy, *J. Am. Ceram. Soc.*, 2001, **84**, 2197.
53 D. Massiot, F. Fayon, M. Capron, I. King, S. Le Calvé, B. Alonso, J.-O. Durand, B. Bujoli, Z. Gan and G. Hoatson, *Magn. Reson. Chem.*, 2002, **40**, 70.
54 R. Jones and J. K. Myers, *J. Organomet. Chem.*, 1972, **34**, C9.
55 M. Weinmann, T. W. Kamphowe, P. Fischer and F. Aldinger, *J. Organomet. Chem.*, 1999, **592**, 115.
56 J. Schuhmacher, PhD thesis, Univ. Stuttgart, 2000.
57 S. Trafl, D. Suttor, G. Motz, E. Rossler and G. Ziegler, *J. Eur. Ceram. Soc.*, 2000, **20**, 215.
58 J. Seitz, J. Bill, N. Egger and F. Aldinger, *J. Eur. Ceram. Soc.*, 1996, **16**, 885.
59 (*a*) G. Jeschke, M. Kroschel and M. Jansen, *J. Non-Cryst. Solids*, 1999, **260**, 216; (*b*) Y. H. Sehlleier, A. Verhoeven and M. Jansen, *J. Mater. Chem.*, 2007, **17**, 4316; (*c*) Y. H. Sehlleier, A. Verhoeven and M. Jansen, *Angew. Chem., Int. Ed.*, 2008, **47**, 3600.
60 G. Schumacher, F. Berger, M. Weinmann, J. Bill, F. Aldinger and K. Muller, *Appl. Organomet. Chem.*, 2001, **15**, 809.
61 F. Berger, A. Müller, F. Aldinger and K. Müller, *Z. Anorg. Allg. Chem.*, 2005, **631**, 355.
62 C. Gervais, F. Babonneau, L. Ruwisch, R. Hauser and R. Riedel, *Can. J. Chem.*, 2003, **81**, 1.
63 S. Duperrier, C. Gervais, S. Bernard, D. Cornu, F. Babonneau and P. Miele, *J. Mater. Chem.*, 2006, **16**, 3126.
64 X. Wu and K. W. Zilm, *J. Magn. Reson., Ser. A*, 1993, **102**, 205.
65 P. Palmas, P. Tekely and D. Canet, *J. Magn. Reson., Ser. A*, 1993, **104**, 26.
66 R. Sangill, N. Rastrup-Andersen, H. Bildsoe, H. J. Jakobsen and N. C. Nielsen, *J. Magn. Reson., Ser. A*, 1994, **107**, 67.
67 L. B. Alemany, D. M. Grant, R. J. Pugmire, T. D. Alger and K. W. Zilm, *J. Am. Chem. Soc.*, 1983, **105**, 2133.
68 N. S. C. K. Yive, R. Corriu, D. Leclercq, P. H. Mutin and A. Vioux, *New J. Chem.*, 1991, **15**, 85.
69 C. Gerardin, F. Taulelle and J. Livage, *MRS Online Proc. LIbr.*, 1993, **287**, 233.
70 W. R. Schmidt, D. M. Narsavage-Heald, D. M. Jones, P. S. Marchetti, D. Raker and G. E. Maciel, *Chem. Mater.*, 1999, **11**, 1455.
71 M. Fontanille and Y. Gnanou, in *Chimie et Physico-chimie des polymères*, Dunod, Paris, 2002.
72 *Calorimetry and Thermal Analysis of Polymers*, ed. V. B. F. Mathot, Hanser, 1994.
73 M. Birot, J. P. Pillot and J. Dunoguès, *Chem. Rev.*, 1995, **95**, 1443.
74 D. D. Edie and M. G. Dunham, *Carbon*, 1989, **27**, 647.

 This journal is © The Royal Society of Chemistry 2012